Eur. Phys. J. D **43**, 27–32 (2007)
DOI: 10.1140/epjd/e2007-00066-0

THE EUROPEAN PHYSICAL JOURNAL D

Model predictions and experimental characterization of Co-Pt alloy clusters

P. Moskovkin[1,a], S. Pisov[1,b], M. Hou[1,c], C. Raufast[2], F. Tournus[2], L. Favre[2,d], and V. Dupuis[2]

[1] Physique des Solides Irradiés et des Nanostructures, CP 234, Université Libre de Bruxelles, Bd du Triomphe, 1050 Bruxelles, Belgium
[2] Laboratoire de Physique de la Matière Condensée et Nanostructures, Université Lyon 1, CNRS UMR 5586, Domaine Scientifique de la Doua, 69622 Villeurbanne Cedex, France

Received 24 July 2006 / Received in final form 3 October 2006
Published online 24 May 2007 –

Abstract. Model and real cobalt-platinum alloy clusters are compared in terms of structure, composition and segregation. Canonical and semi grand canonical Metropolis Monte Carlo simulations are performed to model these clusters, using embedded atom (EAM) and modified embedded atom (MEAM) potentials. All of them correctly predict the bulk $L1_2$ Co_3Pt and $CoPt_3$ structures as well as the $L1_0$ CoPt phase. However, the lattice parameters, phase stability and the $L1_0$-fcc order-disorder transition temperature are at variance. Segregation predictions with EAM and MEAM potentials are contradictory. Experimentally, mixed clusters with various compositions were deposited by Low Energy Cluster Beam on amorphous carbon at room temperature. Their size distribution, crystalline structure and composition were examined by Transmission Electron Microscopy (TEM). Clusters with the same size distributions were modelled. Both experiment and modelling show their crystallographic parameters to continuously correspond to the fcc CoPt chemically disordered phase. Diffraction measurements indicate surface segregation of the specie in excess, in agreement with EAM predictions for the Co-rich phase. The consequences on magnetic properties are discussed.

PACS. 61.46.-w Nanoscale materials

1 Introduction

The study of original magnetic nanogranular structures is playing an increasingly important role directly related with the large number of potential applications in various fields such as information storage and magnetoelectronic devices [1,2]. However when decreasing the size of particles, the *superparamagnetic* behaviour avoids their use as nanomagnet at room temperature. Consequently, a first challenge prior to applications consists to develop novel magnetic materials with a rather high anisotropy in order to remain magnetically oriented up to room temperature or above [1].

Binary alloys with a combination of $3d$ metals and $4d$ or $5d$ materials (such as Pd, Rh, Pt) could probably offer the opportunity to obtain room temperature nanoscale ferromagnet, as related in [1]. Recently, Monte Carlo simulations have been applied to investigate the effects of size and surface segregation on the $L1_0$ ordering in FePt nanoparticles [3]. This has been the starting point of our experimental investigation on Co_xPt_{1-x} clusters prepared by Low Energy Cluster Beam Deposition (LECBD).

Structural properties of Co_3Pt, CoPt and $CoPt_3$ bulk alloys were already studied at the atomic scale [4] by means of Metropolis Monte Carlo (MMC) importance sampling, with special focus on order disorder transitions. In the present study, a similar approach is used, based on a somewhat more general algorithm, with the purpose of emphasizing the role of the cohesion model on thermodynamic, structural and chemical cluster properties. Experimentally, structural observations are reported that can be directly compared to the model and open the way to the assessment of the models.

The present report is organized as follows. Section 2 briefly describes the modelling and the experimental techniques, as well as the model potentials used and their different parameterizations. Section 3 is devoted to the modelling and experimental results. Concluding remarks are presented in Section 4.

[a] *Permanent address*: RRC "Kurchatov Institute", Moscow, Russia.
[b] *Permanent address*: Faculty of Physics, 5 James Bourchier str., 1164 Sofia, Bulgaria.
[c] e-mail: `mhou@ulb.ac.be`
[d] *Present address*: Laboratoire Matériaux et Microélectronique de Provence, UMR CNRS 6137, Université Aix-Marseille 3, 13397 Marseille Cedex 20, France.

2 Modelling and experimental techniques

2.1 Modelling

The general Metropolis Monte Carlo (MMC) algorithm is well documented and the reader is referred to reference [5] for the particular form used here is described in [5]. In the present approach, except when mentioned, the total number of particles of each specie N_{Co} and N_{Pt}, temperature (T) and external pressure (P) — here taken as zero — are fixed, according to the canonical ensemble. This is realistic when particles are synthesized far out of equilibrium conditions, as is the case in laser vaporization environments. For modelling of bulk materials at equilibrium, a fourth kind of trial is used, according to the semi-grand canonical ensemble, on transmuting each atom to the other specie at constant chemical potential difference between them. Typically, two to six millions macro MC steps, each comprising the above mentioned set of trials, are used in order to reach local equilibrium at the atomic scale.

The major model parameter which triggers the equilibrium state of the system is the potential. For metals, many body interactions may be accounted for by means of the Embedded Atom Model. The expression for total energy is written as

$$E_c = \sum_i \left[F(\rho_i) + \frac{1}{2} \sum_{j \neq i} \Phi(R_{ij}) \right]. \tag{1}$$

In this equation ρ_i is a background electron density at the site of atom $i, F(\rho_i)$ is the embedding function, R_{ij} is the distance between atoms i and j, and $\Phi(R_{ij})$ is the pair potential.

We adopt the Co-Pt parameterization in [6,7] accounting for shells of atoms in the contribution to the local electronic density of elemental materials, which turned out to be satisfactory for the AgCo system [8]. In order to use consistent potential cut-offs for Co and Pt, and accounting for the offset from ideal hcp for elemental Co, four first neighbour Pt shells are used with either 9 or 10 shells of Co in its hcp structure. Accordingly, the potential cut-offs used are $1.5a_0(\mathrm{Pt})$ and $1.55a_0(\mathrm{Pt})$ respectively, where $a_0(\mathrm{Pt}) = 0.392$ nm is the Pt equilibrium lattice distance. They will be noted EAM49 and EAM410 in what follows.

The isotropic form of the EAM was implemented with angular dependencies generalized in order to account for possible s, p, d and f hybridizations approximately, leading to the so-called Modified EAM (MEAM). The MEAM model is presented in [9–11] and we only give a brief description here. The range of this potential is limited to first neighbours, considering a screening limiting further neighbours interactions with a suitable screening function [12]. The pair potential is given by

$$\Phi(R_{ij}) = 2\left[E^u(R_{ij}) - F\{\rho(R_{ij})\}\right]/Z \tag{2}$$

where R_{ij} is the distance between atoms i and j, Z is the number of first nearest neighbours in the bulk reference structure (Z =12 in the fcc and tetragonal phases). $E^u(R)$ is the energy per atom of the reference structure, determined according to the equation of Rose [13].

The embedding term for atom i has the form

$$F(\rho_i) = AE_c\rho_i/\rho_0 \ln(\rho_i/\rho_0) \tag{3}$$

A and ρ_0 are parameters which adjustment is given in [9], E_c is the cohesive energy, and ρ_0 is a density scaling parameter.

The electron density ρ_i consists in one isotropic and three angular terms that are described and discussed in [9].

One important point of the model is the definition of the interaction potential between atoms of different kinds. We used the method similar to that described in [9]. It is possible to determine the cross potential based on different reference electronic structures. To this purpose, we choose the $\mathrm{CoPt_3}$ $\mathrm{L1_2}$ and the CoPt $\mathrm{L1_0}$ as reference structures. For the former, the cross potential has the form [14]

$$\begin{aligned}\Phi_{\mathrm{PtCo}}(R) = {} & \frac{1}{3}E^u_{\mathrm{PtCo}}(R) - \frac{1}{4}F_{\mathrm{Pt}}(\overline{\rho}_{\mathrm{Pt}}) \\ & - \frac{1}{12}F_{\mathrm{Co}}(\overline{\rho}_{\mathrm{Co}}) - \Phi_{\mathrm{PtPt}}(R),\end{aligned} \tag{4}$$

where

$$\overline{\rho}_{\mathrm{Co}} = 12\rho^{a(0)}_{\mathrm{Pt}}(R) \tag{5}$$

$$\begin{aligned}\overline{\rho}_{\mathrm{Pt}} = {} & \Bigg(\left(8\rho^{a(0)}_{\mathrm{Pt}}(R) + 4\rho^{a(0)}_{\mathrm{Co}}(R)\right)^2 \\ & + (8/3)t^{(2)}_{\mathrm{Pt}}\left(\rho^{a(2)}_{\mathrm{Pt}}(R) - \rho^{a(2)}_{\mathrm{Co}}(R)\right)^2 \Bigg)^{0.5}\end{aligned} \tag{6}$$

while for the latter, it reads [15]

$$\begin{aligned}\Phi_{\mathrm{PtCo}}(R) = {} & \frac{1}{4}E^u_{\mathrm{PtCo}}(R) - \frac{1}{8}F_{\mathrm{Pt}}(\overline{\rho}^0_{\mathrm{Pt}}) - \frac{1}{8}F_{\mathrm{Co}}(\overline{\rho}^0_{\mathrm{Co}}) \\ & - \frac{1}{4}\Phi_{\mathrm{PtPt}}(R) - \frac{1}{4}\Phi_{\mathrm{CoCo}}(R).\end{aligned} \tag{7}$$

In what follows, the former will be noted MEAM1 and the second MEAM2.

2.2 Experimental

We synthesized mixed $\mathrm{Co}_x\mathrm{Pt}_{1-x}$ clusters (with a target composition: $25 \leqslant x \leqslant 100$ atomic per cent) using the Low Energy Cluster Beam Deposition (LECBD) technique [16]. Neutral clusters were deposited under Ultra High Vacuum on amorphous carbon coated grids, subsequently protected by a thin amorphous silicon layer. Two kinds of samples were prepared: deposits below the 2D-percolation threshold (i.e. discontinuous films of isolated clusters, named: *thin samples)* and after the 2D-percolation threshold (i.e. with coverage rate greater than 50%, named *thick samples*). Cluster size distributions were determined by TEM on the *thin samples* while the shape and atomic structures are evidenced with High resolution TEM measurements. Using electron diffraction and Energy Dispersive X-ray (EDX) spectroscopy on *thick samples*, we relate the stoichiometry and the crystallographic phases.

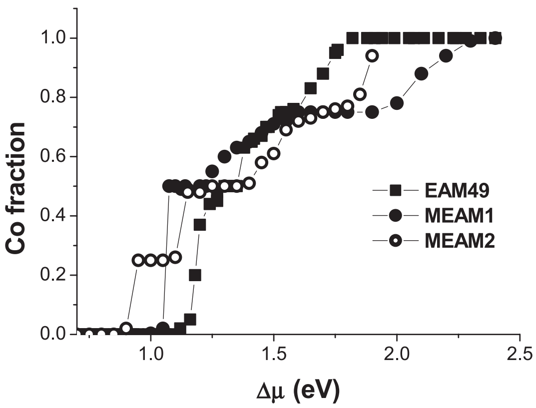

Fig. 1. Dependencies of the Co fraction on the chemical potential difference obtained with the MEAM1, MEAM2 and EAM49 potentials. The isotherms are 300 K. The MEAM potentials predict the correct CoPt and Co_3Pt phases. The $CoPt_3$ ordered phase is only predicted with the MEAM2 potential.

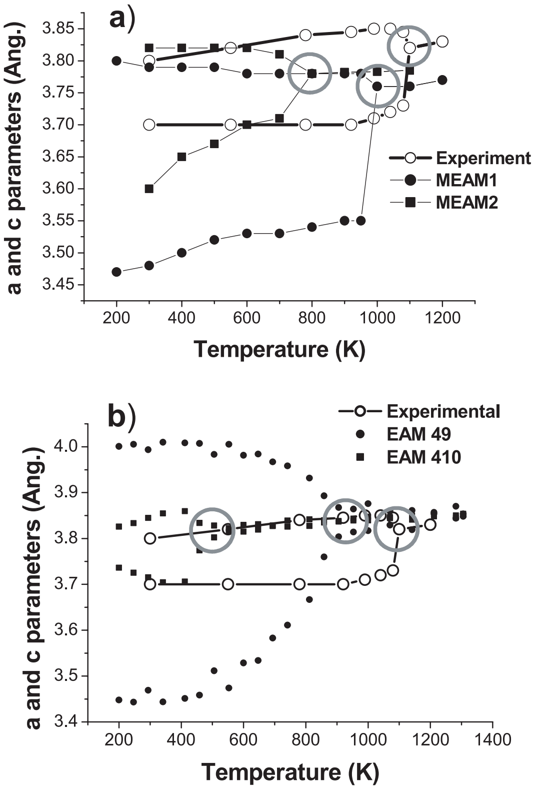

Fig. 2. The temperature dependence of the parameters a and c for the different potential variants used. The predictions are compared with experiment [17]. The OD transitions are referred by a circle and corresponds to the transition from the tetragonal $L1_0$ to the A1 structures.

3 Results

3.1 Modelling results

We now investigate the extent to which the stable bulk phases are predicted by the models. To this purpose, the MC sampling is performed in the semi-grand canonical ensemble ($\Delta\mu$-NPT) in which, thanks to transmutation trials, the composition freely evolves and the equilibrium composition is governed by the fixed chemical potential difference between the Co and the Pt subsystems. Equilibrium compositions are given as functions of $\Delta\mu$ in Figure 1. As previously found in other systems (see e.g. Ref. [5]) ordered phases are predicted stable, corresponding to the plateaus observed in Figure 1. One is the CoPt $L1_0$ phase and the second is the $CoPt_3$ $L1_2$ ordered phase.

The EAM potential only predicts the stable CoPt $L1_0$ phase and fails in predicting the $L1_2$ $CoPt_3$ and Co_3Pt phases; the MEAM2 potential, using CoPt as reference structure (Eq. (4)) is the only one predicting the three phases as stable.

In Figure 2, the parameters a and c of the $L1_0$ tetragonal CoPt crystal are represented as functions of temperature and the values obtained with the four variants of the potentials are compared with diffraction experiment [17]. The MC sampling is achieved in the canonical (NPT) ensemble at zero pressure. An order-disorder transition is clearly observed in the five sets of results, and the transition temperature can be determined. One can see an excellent quantitative agreement between the MEAM1 model (T_{OD} = 1000 K) and experiment (T_{OD} = 1100 K).With the EAM potential, the OD transition temperature is critically dependent on the Co potential, the distance between the 9th and 10th Co neighbours shells being less than 5 percent of the lattice distance. The lattice parameter of the disordered phase predicted by all potential variants is in most reasonable quantitative agreement with experiment. In the ordered phases, predicted lattice parameters do not differ by more than 0.2 Å from experiment.

We now turn to the modelling of clusters. We focus on the cases of CoPt and Co_3Pt clusters containing 500 to 600 atoms, having spherical and truncated octahedral morphologies. These are modelled in the (NPT) ensemble at zero pressure and at a temperature of 300 K. The effect of size and temperature will be commented. In order to determine the structure of the model clusters, it was proceed as follows. As far as the 586 atoms cluster is concerned, $L1_0$ and $L1_2$ order parameters as defined in [18] were measured at 300 K, only taking into account the contribution of atoms that do not sit at the surface. Both CoPt and Co_3Pt clusters were found disordered. Simulations were achieved with the MEAM2 for clusters with all considered compositions and, in no case evidence was found for a tetragonal structure. The predicted dependence of the lattice parameter on the fraction of Co atoms is shown in Figure 3. It is found to decrease with this fraction, which is consistent with the fact that the lattice parameter of bulk fcc Co is smaller than the one of Pt. The results are not found to be significantly size dependent in the range investigated. This indicates that the experimental results may also be little dependent on the cluster size in the same range and that direct comparison is thus possible. Except in the case of pure Co clusters, experimental values overestimate predictions significantly, which is discussed in the next section.

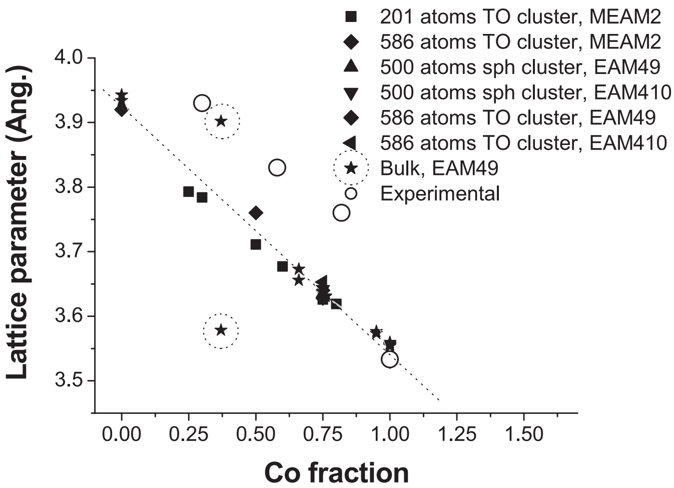

Fig. 3. Predicted and measured lattice parameters as functions of the fraction of Co atoms. All predicted cluster results align on the same linear dependence. Except for compositions allowing the $L1_0$ phase, the same linear dependence is still predicted for the bulk. No tetragonal phase is found in the clusters. The experimental cluster results are above the predicted ones.

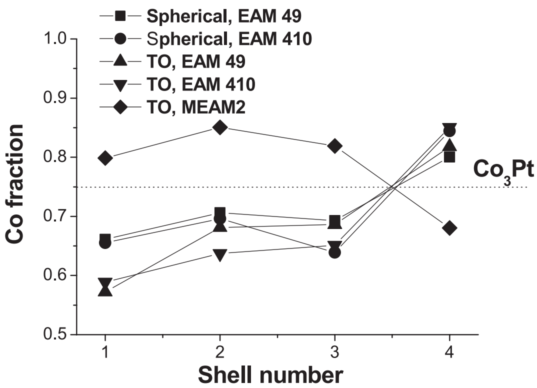

Fig. 4. Fraction of Co atoms in Co_3Pt clusters as a function from the distance from the centre. The temperature is 300 K. The results are not much size dependent. The dotted line indicates the Co_3Pt stoichiometry of the whole cluster.

The segregation state at cluster surfaces is predicted at room temperature for Co_3Pt clusters. One is spherical with 500 atoms and the other is an ideal truncated octahedral cluster with 586 atoms. The calculations were repeated with the EAM49, EAM410 and the MEAM2 potentials. The clusters were subdivided in 4 concentric layers and the fractions of Co atoms obtained are shown in Figure 4. It appears that the radial distributions of the species are different and predicted segregation states are even opposite, depending on the potentials used. Not represented in the figure are the results for MEAM2 in the case of the spherical cluster, where all layers are found stoichiometric. The simulations were repeated at other temperatures and cluster sizes, showing the same potential dependent trends. The two variants of the EAM potential predict a stoichiometry close to CoPt in the core while, with the MEAM2, a similar stoichiometry is predicted in the surface shell. The MEAM2 results correspond to Pt segregation which is found to take place dominantly in the {111} facets of the TO cluster.

This is an example where modeling shows up limitations in the strength of predictions and where experimental assessment is mandatory. The origins of these limitations are multiple and their discussion is beyond the scope of the present paper.

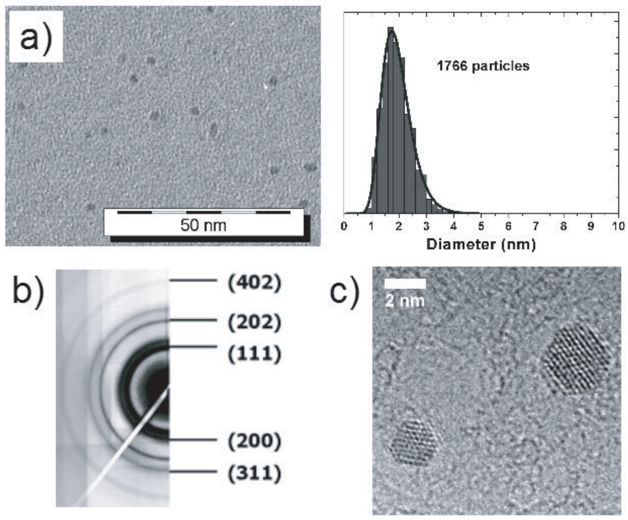

Fig. 5. TEM observation on $CoPt_3$ clusters. (a) Size distributions of deposited $CoPt_3$ clusters. Solid line in the inset represents the best fit of the size distribution obtained using a log-normal function. (b) Electron diffraction on thick $CoPt_3$ samples (c). High Resolution TEM-observations of $CoPt_3$ clusters.

3.2 Experimental results

Collections of supported Co-based clusters present rather narrow size distribution and well-faceted morphology, as shown in Figure 5. From the fits of the size histograms with log-normal functions, we derive the mean diameter D_m and the dispersion σ for thin samples. They are given in Table 1. Systematically, the HRTEM-observations displayed in Figure 5 allow us to conclude that the morphology of Co-based clusters consists on truncated octahedrons crystallized in the fcc-structure corresponding to the equilibrium shape predicted by Wulff [19]. The crystallographic phases are coherent with electron diffraction on 2–3 nm thick clusters films for which we show that the LECBD leads to nanogranular films conserving the crystallographic structure of isolated clusters [20]. For all thin Co_xPt_{1-x} clusters films, the mean clusters diameter has been found as small as 2 nm. These clusters, of truncated-octahedron shape, are made of only a few hundreds of atoms, with a majority located in the first surface layer. From electron diffractions on thick clusters films (see Fig. 5), the intereticular distances d_{111} has been found equal to 2.27, 2.21 and 2.17 Å, respectively with a nominal target concentration $x = 25, 50$ and 75%. In addition,

Table 1. Crystallographic and size distribution characteristics and morphologies of Co-based clusters as deduced from the TEM experiments.

Samples	Crystallographic phases	mean diameter D_m, dispersion σ
Co	One fcc phase with $d_{111} = 2.04$ Å	$D_m = 3.2$ nm, $\sigma = 0.25$
$Co_{0.75}Pt_{0.25}$	One fcc phases with $d_{111} = 2.17$ Å	$D_m = 2.0$ nm, $\sigma = 0.35$
CoPt	One fcc phase with $d_{111} = 2.21$ Å	$D_m = 1.95$ nm, $\sigma = 0.35$
$Co_{0.25}Pt_{0.75}$	One fcc phase with $d_{111} = 2.27$ Å	$D_m = 1.9$ nm, $\sigma = 0.3$

we have performed complementary EDX and RBS analysis in order to determine the real mean composition of the supported Co_xPt_{1-x} clusters films. We observe a systematic enrichment in atomic cobalt concentration compared to the initial target composition, probably due to the laser ablation in our vaporization source, as mentioned in our previous works [21]. The real cobalt composition is the following: 82%, 58% and 30% for a nominal target of 75%, 50% and 25%, respectively.

By keeping in mind that at high temperature and in equilibrium, Co_xPt_{1-x} alloys are continuously soluble and present a face-centred cubic structure for all concentrations [22], in a first approximation, we can use the real atomic clusters concentration in a simple Vegard's law:

$$a_0(\mathrm{Co}_x\mathrm{Pt}_{1-x}) = x\%\ a_0(\mathrm{Co}) + (1-x)\%\ a_0(\mathrm{Pt}) \qquad (8)$$

with $a_0(\mathrm{Co}) = 3.55$ Å and $a_0(\mathrm{Pt}) = 3.93$ Å, to determine the corresponding calculated clusters one. According to (5), $a_0(\mathrm{Co}_x\mathrm{Pt}_{1-x})$ should be equal to 3.62, 3.71 and 3.81 Å for respectively 82%, 58% and 30% real atomic cobalt clusters concentrations. These calculated values are in agreement with the simulation values given in Figure 3 and smaller than the experimental ones. The present systematic relative variation is $\Delta a_0/a_0 \sim -3\%$ for all compositions. By analogy with [23], the variation of the fcc lattice parameter of our Co_xPt_{1-x} samples show the same 2nd Vegard-like linear trend obtained for Fe_xPt_{1-x}, granular systems (and $x > 0.4$) which also present a regular expansion of 3%. Nevertheless for the moment, we are unable to formally conclude about the electron diffraction instrument precision and a possible experimental parameter dilatation in our nanoclusters.

In order to check eventual surface segregations effects in our alloy clusters as identified in the previously studied Co_xPt_{1-x} epitaxial alloys films [24,25], we performed electron diffraction measurements on *thick samples* without silicon coating. For the non-coated $Co_{0.25}Pt_{0.75}$ and $Co_{0.5}Pt_{0.5}$ samples, we identified two phases: one as Co_3O_4 oxide cobalt and an amorphous halo around 2.2 Å which can be related once more to a chemically disordered CoPt phase. For the non-coated CoPt-samples, oxidation is negligible and we retrieve all the rings of the non corrosive A_1 fcc CoPt chemically disordered phase. These results could be in favour of a richer Co shell and a CoPt core in the case of $Co_{0.75}Pt_{0.25}$ clusters. This is consistent with a possible compositional modulation for approximately four monolayers at the surface of Co_xPt_{1-x} alloys [26] and with the EAM simulations in Figure 4. It was suggested in [26] that both the (111) and (100) surfaces are terminated with a pure Pt layer with significant Co enrichment of the second layer. While the (110) surface has the reverse segregation with the surface layer being Co rich and the second one Pt rich. Moreover, magnetization measurements performed on our Co_xPt_{1-x} clusters embedded in MgO and Nb matrices have shown that the higher volume anisotropy K_V has been obtained for $Co_{0.75}Pt_{0.25}$ clusters [27]. Notice that higher magnetocrystalline anisotropy is expected for the $L1_0$ CoPt phase rather than for the $L1_2$ Co_3Pt one. As we obtained the opposite tendency, the origin of such high K_V value could be due to a small chemical CoPt like-ordering in the $Co_{0.75}Pt_{0.25}$ core.

In our case, *one possible model could be that our 2nm small Co_xPt_{100-x} clusters are formed by 3–4 concentric spherical monolayers with surface segregation of the specie in excess.* As found with the EAM potential, in this model, $Co_{75}Pt_{25}$samples should be seen as a CoPt core (counting in average 36% of atoms i.e. 18% of each Co and Pt specie) and a Co shell (with in average 64% of atoms). At the opposite, $Co_{0.25}Pt_{0.75}$samples should be constituted by a core of CoPt (counting 60% of atoms i.e. 30% of each Co and Pt specie) and a Pt shell (with 40% of atoms). To confirm such assumptions, complementary simulations and experiments including in-situ X-ray Photoemission Spectroscopy, He^+ Low Energy Ion Scattering Spectroscopy and HREDX are in progress and will allow further and direct assessment of modelling predictions.

4 Conclusive remarks

Co_xPt_{1-x} clusters were studied in parallel by simulation and experimentally. Cluster structures, lattice distances and segregation states could be characterized independently by the two approaches. Obviously, simulated results depend on the model potential. The sensitivity of predictions on the potential is already evidenced in the bulk CoPt, in particular, as the order-disorder transition is concerned. Order is however neither predicted nor observed in clusters and comparison is satisfactory in several respects. The expected and predicted fcc structure is observed for all compositions. Segregation, which is particularly difficult to measure, still represents an unclear issue. Nevertheless, experiment indicates a possible segregation of the element in excess, favouring a CoPt core in the clusters. Model predictions are contradictory on this point and the less sophisticated potential seems to lead to the predictions the closest to experiment.

A broader set of simulations and of experiments is however needed to settle this question. Work is in progress in order to gather an overall picture of composition distributions in Co-Pt clusters.

Two of us (P.M and S.P.) are grateful the the Fonds National de la Recherche Scientifique of Belgium for grants that allow achieving the present work under contract F.R.S.C. 2.4520.03. The authors are indebted to their colleagues at Lyon: O. Boisron, E. Bernstein and S. Rohart for fruitful discussions and efficient technical assistances during respectively the cluster preparations, TEM-experiments and magnetic measurements. We gratefully acknowledge support from the EU (AMMARE contract N° G5RD-CT 2001-0047P and STREP SFINx N° NMP-CT-2003-505587) for some parts of the work reported in this paper.

References

1. S. Sun, C.B. Murray, D. Weller, L. Folks, A. Moser, Science **287**, 1989 (2000)
2. D.J. Sellmyer, M. Yu, R.D. Kirby, Nanostruct. Mat. **12**, 1021 (1999)
3. B. Yang, M. Asta, O.N. Mryasov, T.J. Klemmer, R.W. Chantrell, Scripta Mat. **53**, 417 (2005)
4. S.I. Park, B.-J. Lee, H.M. Lee, Scripta Mater. **45**, 495 (2001)
5. E.E. Zhurkin, M. Hou, J. Phys.: Condens. Matter **12**, 6735 (2000)
6. R.A. Johnson, Phys. Rev. B **39**, 12554 (1989)
7. A. Johnson, Phys. Rev. B **41**, 9717 (1990)
8. M. Hou, M. El Azzaoui, H. Pattyn, J. Verheyden, G. Koops, G. Zhang, Phys. Rev. B **62**, 5117 (2000)
9. M.I. Baskes, Phys. Rev. B **46**, 2727 (1992)
10. M.I. Baskes, R.A. Johnson, Modell. Simul. Mater. Sci. Eng. **2**, 147 (1994)
11. G. Wang, M.A. Van Hove, P.N. Ross, M.I. Baskes, J. Chem. Phys. **121**, 5410 (2004)
12. M.I. Baskes, Mater. Chem. Phys. **50**, 152 (1997)
13. H. Rose, J.R. Smith, F. Guinea, J. Ferrante, Phys. Rev. B **29**, 2963 (1984)
14. G. Wang, M.A. Van Hove, P.N. Ross, M.I. Baskes, J. Chem. Phys. **121**, 5410 (2004)
15. D. Chen, M. Yan, Y.F. Liu, Sripta Mater. **40**, 913 (1999)
16. A. Perez, P. Mélinon, V. Dupuis, P. Jensen, B. Prével, J. Tuaillon, L. Bardotti, C. Martet, M. Treilleux, M. Broyer, M. Pellarin, J.L. Vialle, B. Palpant, J. Lermé, J. Phys. D Appl. Phys. **30**, 709 (1997)
17. C. Leroux, M.C. Cadeville, V. Pierron-Bohnes, G. Inden, F. Hinz, J. Phys. F **18**, 2033 (1988)
18. P. Moskovkin, M. Hou, J. Alloys Comp. (in press)
19. R. Van Hardeveld, F. Hartog, Surf. Sci. **15**, 189 (1969)
20. L. Favre, V. Dupuis, E. Bernstein, S. Stanescu, P. Mélinon, A. Perez, T. Epicier, J.P. Simon, J.M. Tonnerre, D. Babonneau, Phys. Rev. B **74**, 014439 (2006)
21. V. Dupuis, M. Jamet, J. Tuaillon-Combes, L. Favre, S. Stanescu, M. Treilleux, E. Bernstein, P. Mélinon, A. Perez, *Review of "Recent research Developments in Magnetism and Magnetic Materials"* **1**, (2003) 101 Transworld Research Network
22. M. Hansen, K. Anderko, *Constitution of Binary Alloys* (McGraw-Hill, New York, 1958), pp. 467, 516
23. A. Bonakdarpour et al., J. Electrochem. Soc. **152**, A61 (2005)
24. M. Maret, M.C. Cadeville, W. Staiger, E. Beaurepaire, R. Poinsot, A. Herr, Thin Solid Film **275**, 224 (1996)
25. M. Maret, M.C. Cadeville, R. Poinsot, A. Herr, E. Beaurepaire, C. Monier, J. Mag. Mag. Mat. **166**, 45 (1997)
26. A.I. Shapiro, P.W. Rooney, M.Q. Tran, F. Hellman, K.M. Ring, K.L. Kavanagh, B. Rellinghauss, D. Weller, Phys. Rev. B **60**, 12826 (1999)
27. S. Rohart, C. Raufast, L. Favre, E. Bernstein, E. Bonet-Orozco, V. Dupuis, Phys. Rev. B **74**, 104408 (2006)